SCIENCE CHINA
Life Sciences

•RESEARCH PAPER•

November 2022 Vol.65 No.11: 2233–2247
https://doi.org/10.1007/s11427-021-2089-8

Circular RNA *circCCNB1* inhibits the migration and invasion of nasopharyngeal carcinoma through binding and stabilizing *TJP1* mRNA

Mengyao Zhao[1,2†], Yian Wang[1,2†], Fenghua Tan[2], Lingyun Liu[3], Xiangchan Hou[2], Chunmei Fan[2], Le Tang[2], Yongzhen Mo[2], Yumin Wang[2], Qijia Yan[2], Zhaojian Gong[4], Zheng Li[2], Qianjin Liao[1], Can Guo[2], He Huang[2], Xi Zeng[3], Guiyuan Li[1,2,5], Zhaoyang Zeng[1,2], Wei Xiong[1,2*] & Fuyan Wang[2*]

[1]*NHC Key Laboratory of Carcinogenesis, Hunan Cancer Hospital and the Affiliated Cancer Hospital of Xiangya School of Medicine, Central South University, Changsha 410078, China;*
[2]*Key Laboratory of Carcinogenesis and Cancer Invasion of the Chinese Ministry of Education, Cancer Research Institute, Central South University, Changsha 410083, China;*
[3]*Cancer Research Institute, Hengyang Medical College, University of South China, Hengyang 421009, China;*
[4]*Department of Oral and Maxillofacial Surgery, the Second Xiangya Hospital, Central South University, Changsha 410011, China;*
[5]*Hunan Key Laboratory of Nonresolving Inflammation and Cancer, Disease Genome Research Center, the Third Xiangya Hospital, Central South University, Changsha 410013, China*

Received November 7, 2021; accepted March 12, 2022; published online April 21, 2022

Nasopharyngeal carcinoma (NPC) is a malignant tumor that usually occurs in people from Southeast Asia and Southern China. NPC is prone to migration and invasion, leading to poor prognosis. A large number of circular RNAs (circRNAs) exacerbate the process of metastasis in NPC; however, their underlying mechanisms remain unclear. We found that the circular RNA *circCCNB1*, encoded by the oncogene *CCNB1*, was downregulated in NPC biopsies and cell lines. *In vitro* assays show that *circCCNB1* inhibits NPC cell migration and invasion. Moreover, *circCCNB1* induces a protein, nuclear factor 90 (NF90), to bind and prolong the half-life of tight junction protein 1 (*TJP1*) mRNA. Upregulation of TJP1 enhances tight junctions between cancer cells and inhibits NPC cell migration and invasion. This study reveals a novel biological function of *circCCNB1* in the migration and invasion of NPC by enhancing the tight junctions of cancer cells by binding to NF90 proteins and *TJP1* mRNA, and may provide a potential therapeutic target for NPC.

nasopharyngeal carcinoma, *circCCNB1*, NF90, *TJP1*, migration and invasion

Citation: Zhao, M., Wang, Y., Tan, F., Liu, L., Hou, X., Fan, C., Tang, L., Mo, Y., Wang, Y., Yan, Q., et al. (2022). Circular RNA *circCCNB1* inhibits the migration and invasion of nasopharyngeal carcinoma through binding and stabilizing *TJP1* mRNA. Sci China Life Sci 65, 2233–2247. https://doi.org/10.1007/s11427-021-2089-8

INTRODUCTION

Nasopharyngeal carcinoma (NPC) is the most common malignant tumor of the head and neck in Southeast Asia and Southern China and originates from the epithelial tissue of the nasopharynx (Wang et al., 2022c; Zeng et al., 2011). Etiological studies have shown that carcinogenesis of NPC is related to genetic (Jiang et al., 2022) and environmental factors (Hildesheim and Wang, 2012). Chemical substances

†Contributed equally to this work
*Corresponding authors (Wei Xiong, email: xiongwei@csu.edu.cn; Fuyan Wang, email: wfy4010@csu.edu.cn)

(Aussem et al., 2012), such as nitrite and Epstein-Barr virus (EBV) (Ge et al., 2021; Wang et al., 2022a; Wu et al., 2020b) are the major environmental factors. Most NPCs are non-keratinizing cancers (Zhao et al., 2020), which are prone to migration and invasion (Xiong et al., 2021). Since the early symptoms of NPC are atypical, most patients are diagnosed after having lymph node or distant metastasis. The prognoses of late-stage patients are relatively poor (Fan et al., 2021b; Mo et al., 2021). Therefore, exploring the molecular mechanism of NPC migration and invasion and identifying novel molecular markers or targets are very important for the early diagnosis and treatment of NPC (Fan et al., 2020; Fan et al., 2019; Qu et al., 2021; Qu et al., 2022; Ren et al., 2020; Zhu et al., 2021).

Circular RNAs (circRNAs) have a closed circular structure and are widely expressed in mammalian cells (Wang et al., 2022b). Although they used to be considered as the "waste" of RNA splicing over the last century (Ouyang et al., 2021a; Ouyang et al., 2021b; Sanger et al., 1976), in recent years, with the development of next-generation sequencing technology, an increasing number of studies have demonstrated that circRNAs are related to many human diseases (Xie et al., 2018; Zhong et al., 2018; Zhu et al., 2019), especially malignant tumors (Fan et al., 2021a; Li et al., 2021; Saw et al., 2021; Tang et al., 2021; Wang et al., 2020; Wu et al., 2020a; Zhou et al., 2018). Some well-known oncogenes or tumor suppressor genes can also encode circRNAs, which may play important roles in coordinating or antagonizing host genes in cancer progression. For example, *circβ-catenin*, a circular RNA encoded by the oncogene *β-catenin*, can promote malignant progression of liver cancer by activating the Wnt signaling pathway (Liang et al., 2019). *circAKT3* derived from the oncogene *AKT* can inhibit the malignant progression of glioblastoma by encoding a small peptide (Xia et al., 2019), while *circ-E-Cad* derived from the tumor suppressor gene *E-cadherin* can promote the development of glioblastoma by encoding a small peptide (Gao et al., 2021). However, the function of circRNAs in NPC has not yet been sufficiently studied.

In this study, we found that a circular RNA, *circCCNB1*, which is derived from the oncogene *CCNB1*, was downregulated in NPC and inhibited NPC cell migration and invasion. We revealed that *circCCNB1* can bind to the nuclear factor 90 (NF90) protein and tight junction protein 1 (*TJP1*) mRNA simultaneously, enhancing *TJP1* mRNA stability and upregulating TJP1 protein, ultimately inhibiting NPC migration and invasion.

RESULTS

circCCNB1 is downregulated in NPC

There are two alternative splice forms of circular RNAs derived from the *CCNB1* gene, named *circCcnb1*, formed by exons 4 and 5 of *CCNB1* (Fang et al., 2018; Fang et al., 2019), and *circCCNB1*, formed by exons 6 and 7 (Yu et al., 2019). However, their expression and function in NPCs have not been investigated. The expression of *circCcnb1* and *circCCNB1* (Figure 1A) was examined in NPC tissues (Table S1 in Supporting Information) and cell lines. The data showed that *circCCNB1* was significantly downregulated in NPC biopsies and cell lines compared to that in normal controls (Figure 1B and C). Since the expression of *circCcnb1* was extremely low or not detected in either NPC samples or normal controls (data not shown), we recommend *circCCNB1* for further investigation. RNase R treatment followed by real-time quantitative polymerase chain reaction (RT-qPCR) showed *circCCNB1* was resistant to RNase R exonuclease digestion owing to its circular conformation (Figure 1D). The half-life of *circCCNB1* was longer than that of *CCNB1* mRNA in NPC cells after actinomycin D treatment (Figure 1E).

circCCNB1 inhibits NPC migration and invasion.

Small interfering RNA (siRNA) targeting the back-splicing site of *circCCNB1* was designed, and the overexpression vector of *circCCNB1* was constructed, to identify the function of *circCCNB1* in NPC. Splice forms were transfected into their respective NPC cell lines (Figure S1A in Supporting Information). Since *CCNB1* is an important oncogene that can promote the cell cycle, the function of *circCCNB1* in the proliferation of NPC cells was first measured using MTT (3-(4,5-dimethylthiazol-2-yl)-2,5-diphenyltetrazolium bromide) and clone formation assays. Knockdown or overexpression of *circCCNB1* had no effect on NPC cell proliferation (Figure S1B and C in Supporting Information). Wound healing and transwell assay results showed that the migration and invasion speed of NPC cells was significantly faster after knockdown of *circCCNB1* and slower after overexpression, compared with the negative control (Figure 2A and B). These findings suggest that *circCCNB1* may function as a tumor suppressor gene in NPC by inhibiting the migration and invasion of NPC cells.

circCCNB1 improves *TJP1*'s stability through binding with its mRNA

To explore the mechanism of *circCCNB1* on the migration and invasion inhibition of NPC cells, we constructed differential proteomic expression profiles in HNE2 cells after knockdown or overexpression of *circCCNB1* using high-throughput liquid chromatography-tandem mass spectrometry (LC-MS; Figure S2A in Supporting Information). Thirty proteins were positively regulated and 22 proteins were negatively regulated by *circCCNB1* (Figure S2B and Table S2 in Supporting Information). Among them, many

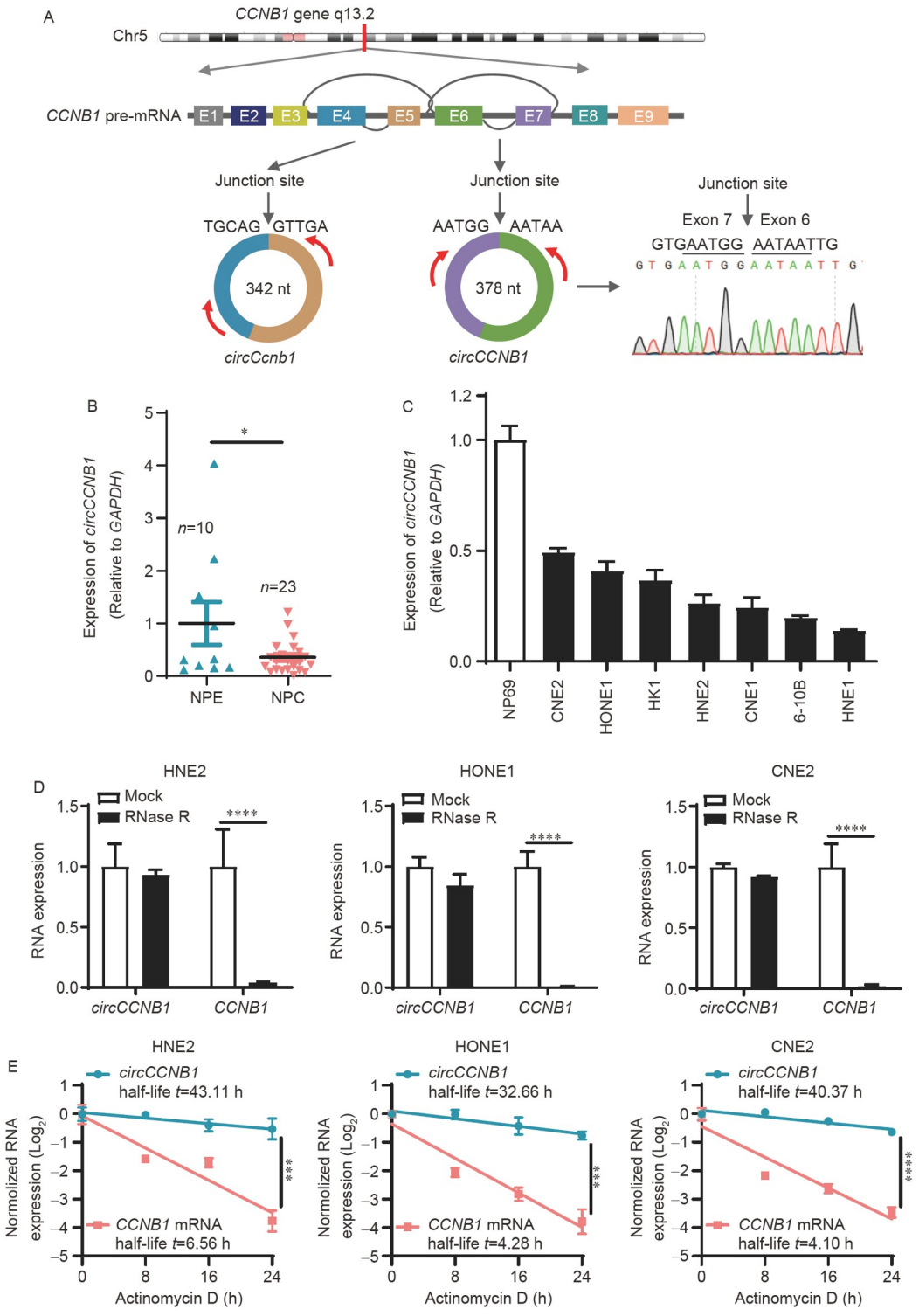

Figure 1 *circCCNB1*, back-spliced from exon 6 and 7 of *CCNB1*, is downregulated in NPC. A, There are two forms of circRNAs (*circCCNB1* and *circCcnb1*) derived by *CCNB1* pre-mRNA. *circCcnb1* (342 nt) is composed by exons 4 and 5 while *circCCNB1* (378 nt) is formed by exons 6 and 7. Sanger sequencing was used to confirm that *circCCNB1* was the major circular transcript of the *CCNB1* gene. B, RT-qPCR was used to analyze the expression of *circCCNB1* in 10 non-cancerous nasopharyngeal epithelial (NPE) and 23 NPC tissues. *circCCNB1* was significantly down-regulated in NPC biopsies. (*, $P<0.05$). C, RT-qPCR analyzed the expression of *circCCNB1* in NPC cell lines including CEN2, HONE1, HK1, HNE2, CNE1, 6-10B, and HNE1, and the immortalized nasopharyngeal epithelial cells, NP69, was used as normal control. *circCCNB1* was also expressed at significantly lower levels in NPC cell lines. D, Total RNAs extracted from three NPC cells (HNE2, HONE1, and CNE2) were treated by RNase R for 30 min, and then reverse-transcribed. The relative content of *circCCNB1* and *CCNB1* mRNA were detected by RT-qPCR. *circCCNB1* was more stable and resistance to RNase R. (****, $P<0.0001$). E, The relative expression levels of *circCCNB1* and *CCNB1* mRNA were detected in three NPC cells (HNE2, HONE1, and CNE2) after actinomycin D treatment for 0, 8, 16, and 24 h.*circCCNB1* had longer half-life time than *CCNB1* mRNA. The vertical axis is log and all data were normalized using $\log_2$. (***, $P<0.001$; ****, $P<0.0001$)

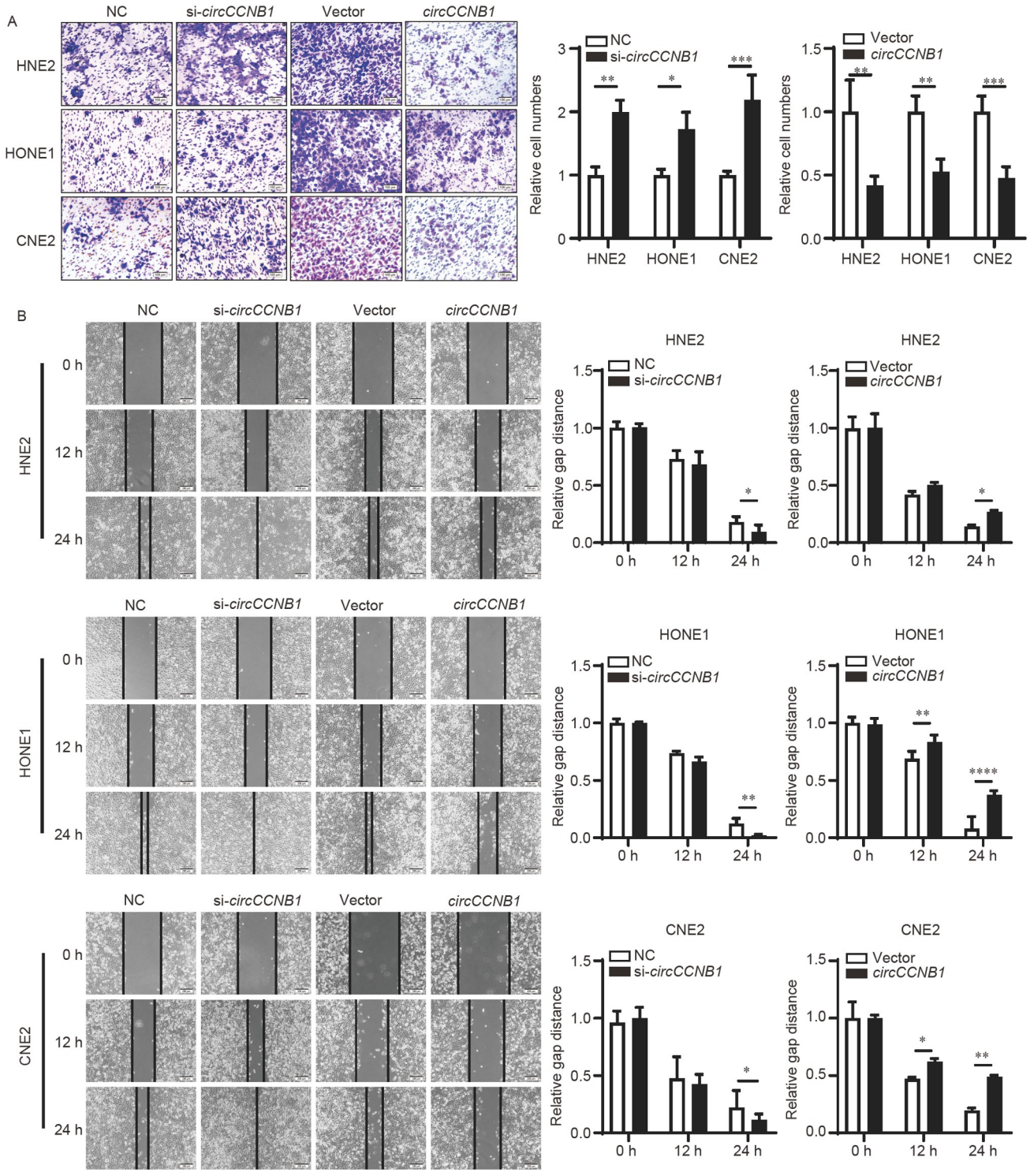

Figure 2 *circCCNB1* inhibits NPC cell migration and invasion. A, The invasive capability was assessed in NPC cells HNE2, HONE1, and CNE2, after knockdown or overexpression of *circCCNB1* by transwell assay. (*, P<0.05; **, P<0.01; ***, P<0.001). B, The migration capability was assessed in HNE2, HONE1, and CNE2 cells after knockdown or overexpression of *circCCNB1* by wound healing assay. (*, P<0.05; **, P<0.01; ****, P<0.0001) ..

proteins are closely related to cell-cell adhesion pathways, including TJP1, LASP1, IDH1, ACTR3, CTTN, PCBP1, RANGAP1, S100A11, SH3GL1, and MYL12A, according to the Metascape and David databases (Figure S2C in Supporting Information).

circRNAs may function as competing endogenous RNAs (ceRNAs) to regulate target mRNA expression. We doubted whether *circCCNB1* could regulate these cell-cell adhesion-related genes at the mRNA level, and their expression was examined in NPC cells after knockdown or overexpression

of *circCCNB1* by RT-qPCR. Only *TJP1* mRNA was significantly downregulated after knockdown of *circCCNB1* and upregulated after overexpression of *circCCNB1* (Figure 3A), while the other mRNAs, including *LASP1* and *CTTN*, showed no obvious changes after knockdown or overexpression of *circCCNB1* (Figure S3A in Supporting Information). Western blotting results also confirmed that *circCCNB1* could upregulate TJP1 protein expression (Figure 3B). The expression of *TJP1* mRNA in NPC tissues and cell lines was also measured using RT-qPCR. The results showed that *TJP1* mRNA was also downregulated in NPC tissues and cell lines (Figure S3B in Supporting Information) and positively correlated with *circCCNB1* expression (Figure S3C in Supporting Information).

However, the RegRNA2.0 software showed that there are no miRNAs that target both *circCCNB1* and the *TJP1* 3′-untranslated region (UTR), indicating that *circCCNB1* may not regulate *TJP1* through the ceRNA mechanism. Interestingly, the RNAhybrid software showed that *circCCNB1* may bind to the *TJP1* 3′UTR directly (Figure 3C). The circRNA immunoprecipitation (circRIP) assay verified the combination of *circCCNB1* and *TJP1* 3′UTR using biotin-labeled *circCCNB1* (Figure 3D). The 3′UTR is important for maintaining mRNA stability (Karthi et al., 2017; Ouhara et al., 2018). Actinomycin D treatment followed by RT-qPCR showed that *TJP1* mRNA stability was significantly decreased in NPC cells after knockdown of *circCCNB1*, while overexpression of *circCCNB1* had an opposite effect on *TJP1* mRNA stability (Figure 3E). These results indicate that *circCCNB1* can directly bind to *TJP1* mRNA to improve its stability in NPC cells.

TJP1, also named ZO-1 (zonula occludens 1), acts as a tight junction adaptor protein that provides a link between occludin, a transmembrane tight junction protein, and the actin cytoskeleton (Runkle and Mu, 2013; Zhang et al., 2018). To identify the function of TJP1 in NPC, we performed transwell and wound healing assays, which showed that knockdown of TJP1 (Figure 4A and B) promoted NPC cell migration and invasion, and reversed the inhibitory effect of *circCCNB1* on migration and invasion (Figure 4C and D). These results demonstrated that *circCCNB1* stabilized the expression of *TJP1* by binding to its 3′UTR region, which increased the expression of TJP1 and inhibited NPC cell migration and invasion.

circCCNB1 increases *TJP1* mRNA stability through enhancing the binding of *TJP1* mRNA and NF90 protein

To explore whether there is a protein that participates in the regulation of *TJP1* mRNA stability, we performed an RNA pull-down assay using biotin-labeled *circCCNB1* followed by LC-MS, and identified a total of 276 proteins (Figure 5A; Figure S4A and Table S3 in Supporting Information). Nine potential *circCCNB1* binding proteins were predicted using both the circAtlas and RBPsuite databases (Figure S4B in Supporting Information). The interleukin enhancer binding factor 3 (ILF3), also named NF90, was selected because its high score of prediction and it was reported to play an important role in RNA metabolism via bind to a variety of RNAs and regulate their expression (Ye et al., 2017). RNA pull-down and RNA-binding protein immunoprecipitation (RIP) assays verified that *circCCNB1* and NF90 could bind to each other (Figure 5B and C). Fluorescence *in situ* hybridization (FISH) and immunofluorescence (IF) assays also showed that *circCCNB1* and NF90 co-localized mainly in the cell nucleus (Figure 5D).

It has been reported that NF90 can affect dozens of mRNA stability (Ao et al., 2020; Jiang et al., 2015; Song et al., 2017), translation (Kuwano et al., 2010), and transportation (Ding et al., 2020) by binding to them. To determine whether NF90 binds to *TJP1* mRNA and affects its stability, we performed an RIP assay, and the data showed that NF90 could also bind to *TJP1* mRNA in NPC cells using an anti-NF90 antibody (Figure S5A in Supporting Information). We used the RBPsuite database to predict the binding site of NF90 to *TJP1* mRNA. The predicted results showed that NF90 was most likely to bind to the *TJP1* mRNA 6,651–6,720 nt (site 1) segment, while it was least likely to bind to the *TJP1* mRNA 4,621–4,690 nt (site 2) (Figure S5B in Supporting Information). We used site 2 with the lowest binding potential as a negative control, and the results of RIP experiments showed that NF90 binds to the *TJP1* mRNA 6,651–6,720 nt segment exactly (Figure S5C in Supporting Information). Knockdown or overexpression of NF90 in NPC cells dramatically downregulated or upregulated TJP1 expression, respectively (Figure S5D and E in Supporting Information). Actinomycin D treatment followed by RT-qPCR showed that knockdown of NF90 promoted the degradation of *TJP1* mRNA, while overexpression of NF90 inhibited its degradation (Figure S5F in Supporting Information).

When *circCCNB1* was knockdown in NPC cells, the RIP assay showed that the binding ability between NF90 and *TJP1* mRNA decreased while *circCCNB1* overexpression increased this binding ability (Figure 6A). Overexpression or knockdown of NF90 partially reversed the regulation of knockdown or overexpression of *circCCNB1* on *TJP1* expression (Figure 6B and C). Actinomycin D treatment of NPC cells confirmed that NF90 participates in the regulation of *TJP1* mRNA stability regulated by *circCCNB1* (Figure 6D). Transwell and wound healing assays further confirmed that NF90 could partially promote the function of *circCCNB1* in the migration and invasion of NPC (Figure 7A and B; Figure S6 in Supporting Information). Furthermore, we examined the effects of *circCCNB1* and NF90 on metastatic markers. Knockdown of *circCCNB1* down-regulated the expression of E-cadherin while upregulating the ex-

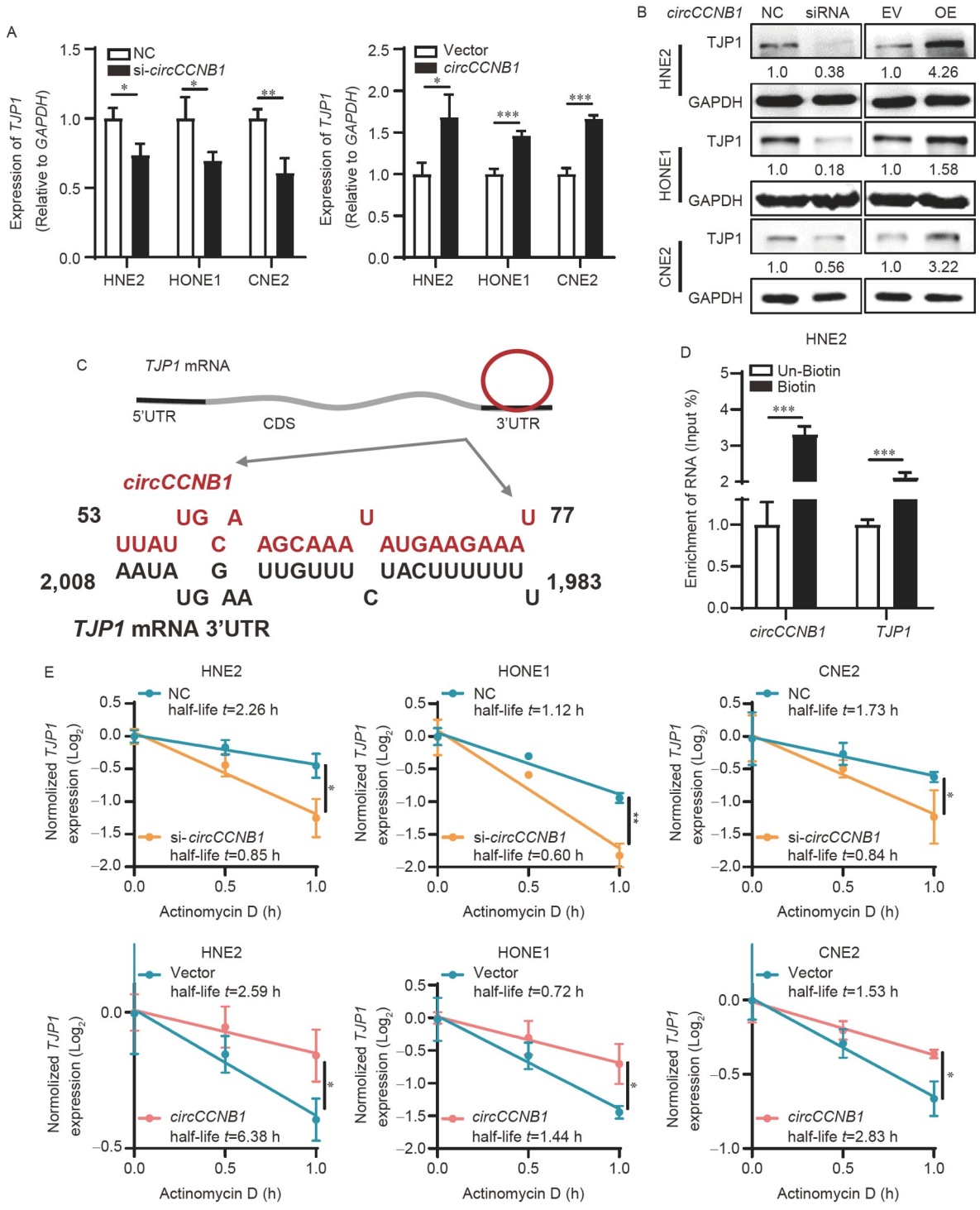

Figure 3 *circCCNB1* can bind to the *TJP1* mRNA and enhance its stability. A, RT-qPCR analysis of the *TJP1* expression in HNE2, HONE1, and CNE2 cells after knockdown or overexpression of *circCCNB1*. (*, $P<0.05$; **, $P<0.01$; ***, $P<0.001$). B, Western blotting analysis the TJP1 expression in HNE2, HONE1, and CNE2 cells after knockdown or overexpression of *circCCNB1*. C, Schematic diagram of the binding between *circCCNB1* and *TJP1* mRNA 3′ UTR. D, circRIP assay confirmed that *circCCNB1* bind to *TJP1* mRNA 3′UTR. (***, $P<0.001$). E, The *TJP1* mRNA expression was detected in HNE2, HONE1, and CNE2 cells after knockdown or overexpression of *circCCNB1* after actinomycin D treatment for 0, 0.5, and 1 h by RT-qPCR. The vertical axis is log and all data were normalized using $\log_2$. (*, $P<0.05$; **, $P<0.01$).

pression of N-cadherin, MMP9 and Claudin-1. Overexpression of NF90 counteracted the effects of knockdown of *circCCNB1* on these metastasis markers, while overexpression of *circCCNB1* then knockdown of NF90 showed the opposite results (Figure 7C). Collectively, these results suggest that *circCCNB1* maintains the stability of *TJP1* mRNA by inducing the binding of NF90 to *TJP1* mRNA, thereby hindering the migration and invasion of NPC.

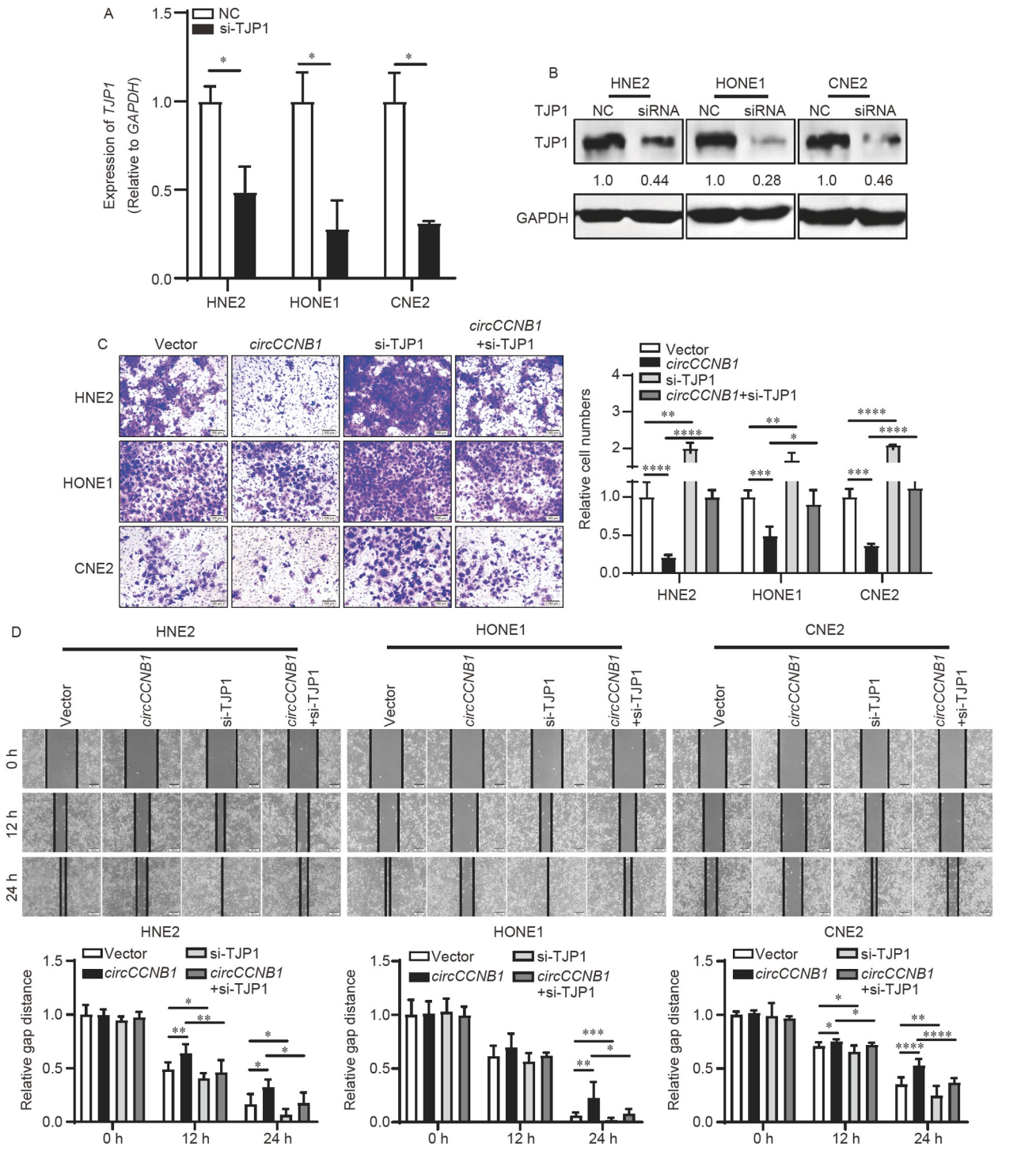

Figure 4 *circCCNB1* inhibits the migration and invasion of NPC through TJP1. A, The knockdown efficiency of TJP1 siRNA was examined in NPC cells HNE2, HONE1, and CNE2 by RT-qPCR. (*, P<0.05). B, The knockdown efficiency of TJP1 siRNA was examined in NPC cells HNE2, HONE1, and CNE2 by Western blotting. C, The invasive capability was assessed in HNE2, HONE1, and CNE2 cells co-transfected with the *circCCNB1* overexpression vector and TJP1 siRNA by transwell assays. (*, P<0.05; **, P<0.01; ***, P<0.001; ****, P<0.0001). D, The migration capability was assessed in HNE2, HONE1, and CNE2 cells co-transfected with the *circCCNB1* overexpression vector and TJP1 siRNA by wound healing assays. (*, P<0.05; **, P<0.01; ***, P<0.001; ****, P<0.0001) .

DISCUSSION

CCNB1, a member of the cyclin family, participates in cell cycle regulation and plays an important role in the occurrence and development of tumors (Chen et al., 2019; Xie et al., 2020). *CCNB1* includes nine exons and can form a variety of circRNAs, of which two circular forms have been reported (Fang et al., 2018; Fang et al., 2019; Yu et al., 2019).

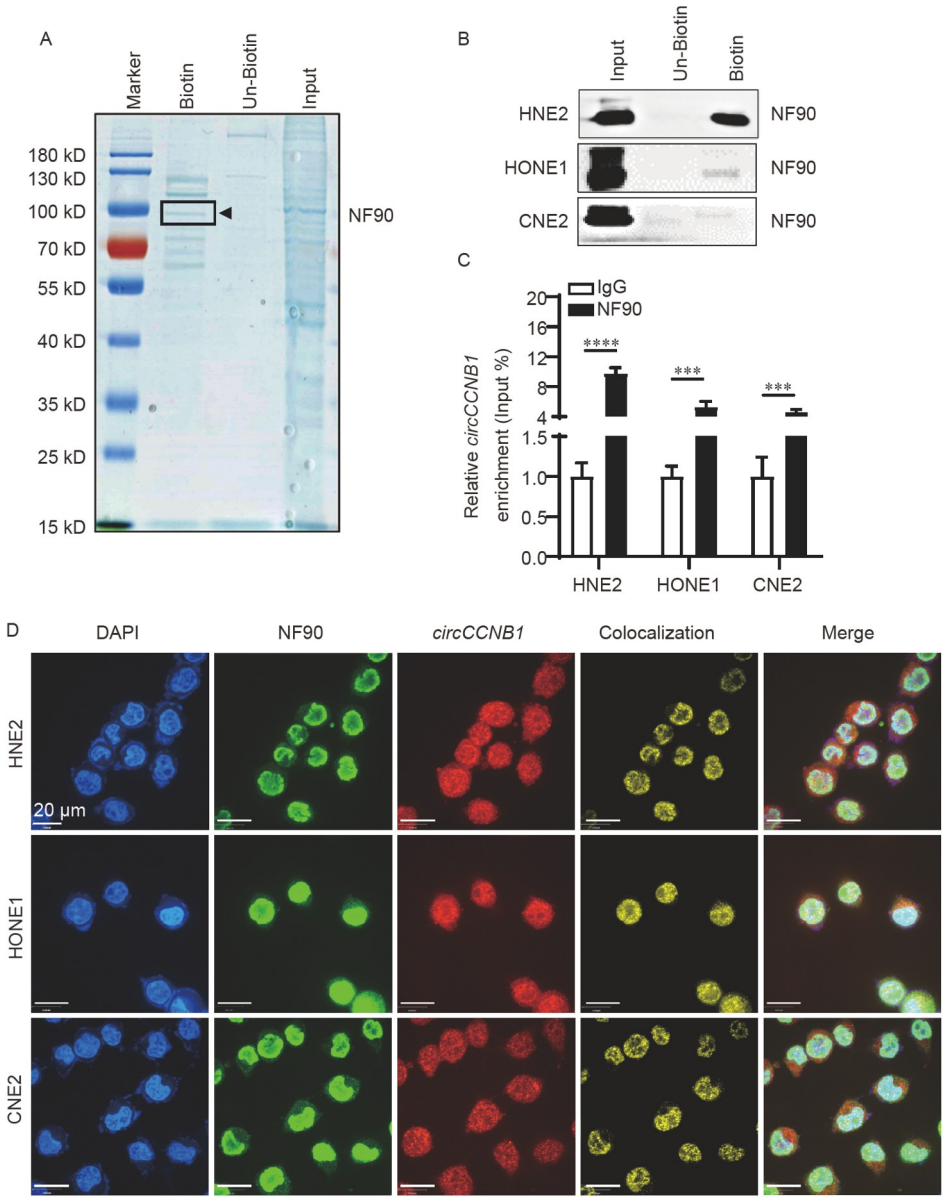

Figure 5 *circCCNB1* can interact with NF90. A, RNA pull-down assay followed by Coomassie blue staining was performed showed that the binding proteins of *circCCNB1*, including NF90. B, RNA pull-down followed Western blotting showed that the interaction between *circCCNB1* and NF90. C, RIP assay verified the interaction between *circCCNB1* and NF90. (***, $P<0.001$; ****, $P<0.0001$). D, FISH and IF assays were performed to verify the co-localization of *circCCNB1* and NF90 in NPC cells. Scale bar=20 μm.

The first is *circCcnb1*, formed by exons 4 and 5 of *CCNB1*, which was reported to inhibit tumor progression caused by p53 mutations in human breast cancer (Fang et al., 2018). *circCcnb1* can also bind to CCNB1 and cyclin-dependent kinase 1 (CDK1) proteins to depolymerize the CCNB1/CDK1 complex. Consequently, CCNB1 loses its role in promoting the invasion, migration, and proliferation of breast cancer cells (Fang et al., 2019). The other is *circCCNB1*, which was previously reported as a sponge of miR-449a to delay cellular senescence by targeting CCNE2 (Yu et al., 2019).

In this study, we found that *circCCNB1* was expressed at low levels in NPC tissues. The expression of *circCcnb1* in NPC was also examined, with minimal detection in NPC clinical samples. We demonstrated that *circCCNB1* inhibited NPC migration and invasion by promoting the binding between NF90 and *TJP1* mRNA, stabilizing *TJP1* mRNA, and enhancing tight junctions between tumor cells.

TJP1 is a critical regulator of tight junction assembly that regulates adherens junction function by coordinating the assembly or dynamics of the cortical cytoskeleton (Mattern et al., 2019). Epithelial-mesenchymal transition (EMT) is the first step in cancer metastasis and involves the reorganization of cell-cell adhesion complexes, including adherens and tight

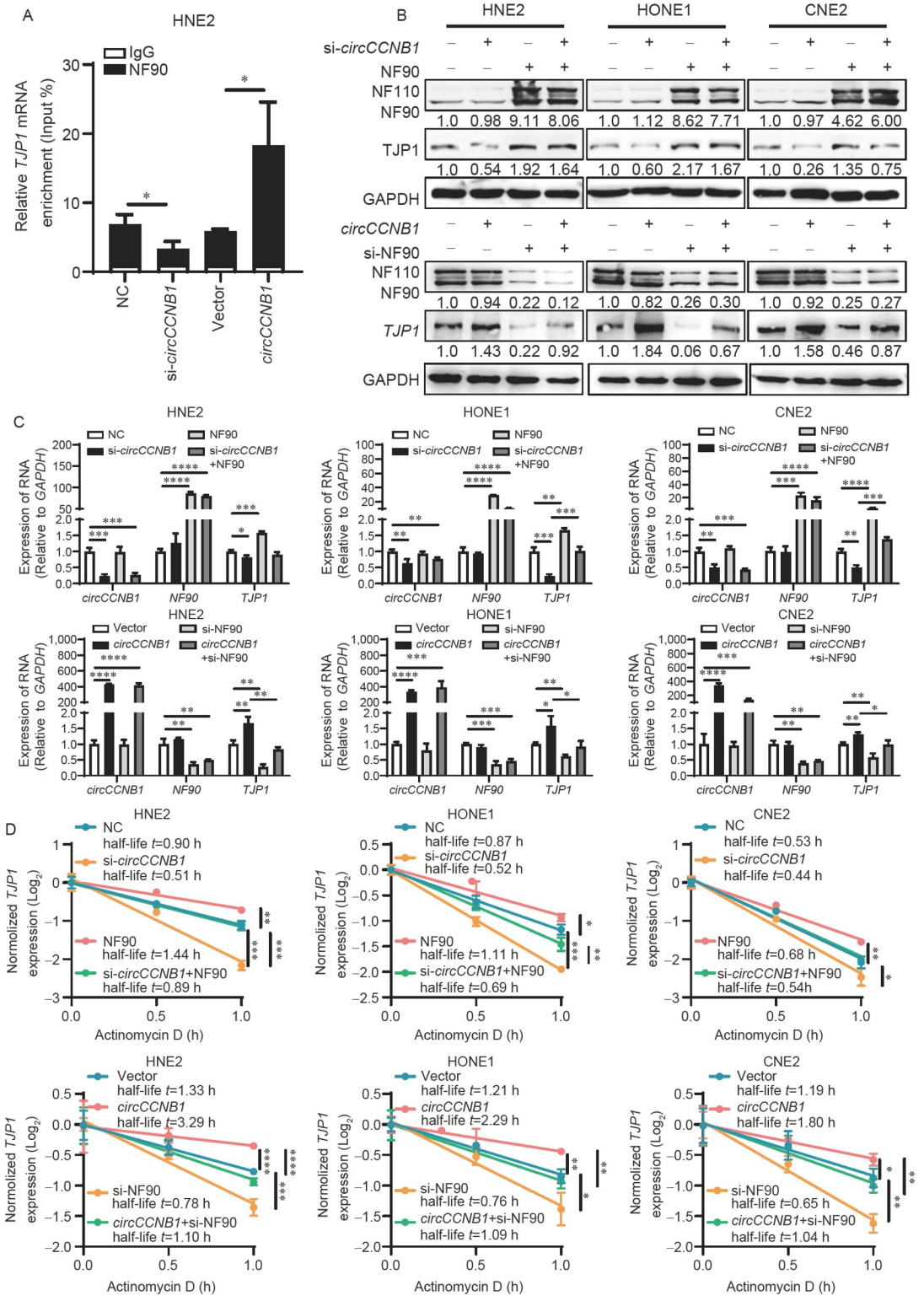

Figure 6 *circCCNB1* stabilizes the *TJP1* mRNA through promoting the binding of *TJP1* mRNA and NF90 protein. A, RIP assays showed that knockdown of *circCCNB1* significantly decreased the interaction between NF90 and *TJP1* mRNA, while overexpression of it increased their interaction. (*, P<0.05). B, Western blotting analysis showed that NF90 participated in the regulation of TJP1 protein by *circCCNB1* in NPC cells after co-transfection the *circCCNB1* siRNA and NF90 overexpression vector, or co-transfection the overexpression vector of *circCCNB1* and NF90 siRNA. C, RT-qPCR analysis showed that NF90 participated in the regulation of *TJP1* mRNA by *circCCNB1* in NPC cells after co-transfection the *circCCNB1* siRNA and NF90 overexpression vector, or co-transfection the overexpression vector of *circCCNB1* and NF90 siRNA. (*, P<0.05; **, P<0.01; ***, P<0.001; ****, P<0.0001). D, The *TJP1* mRNA was detected in NPC cells after co-transfection the *circCCNB1* siRNA and NF90 overexpression vector, or co-transfection the overexpression vector after actinomycin D treatment for 0, 0.5, and 1 h by RT-qPCR. The vertical axis is log and all data were normalized using $\log_2$. (*, P<0.05; **, P<0.01; ***, P<0.001; ****, P<0.0001).

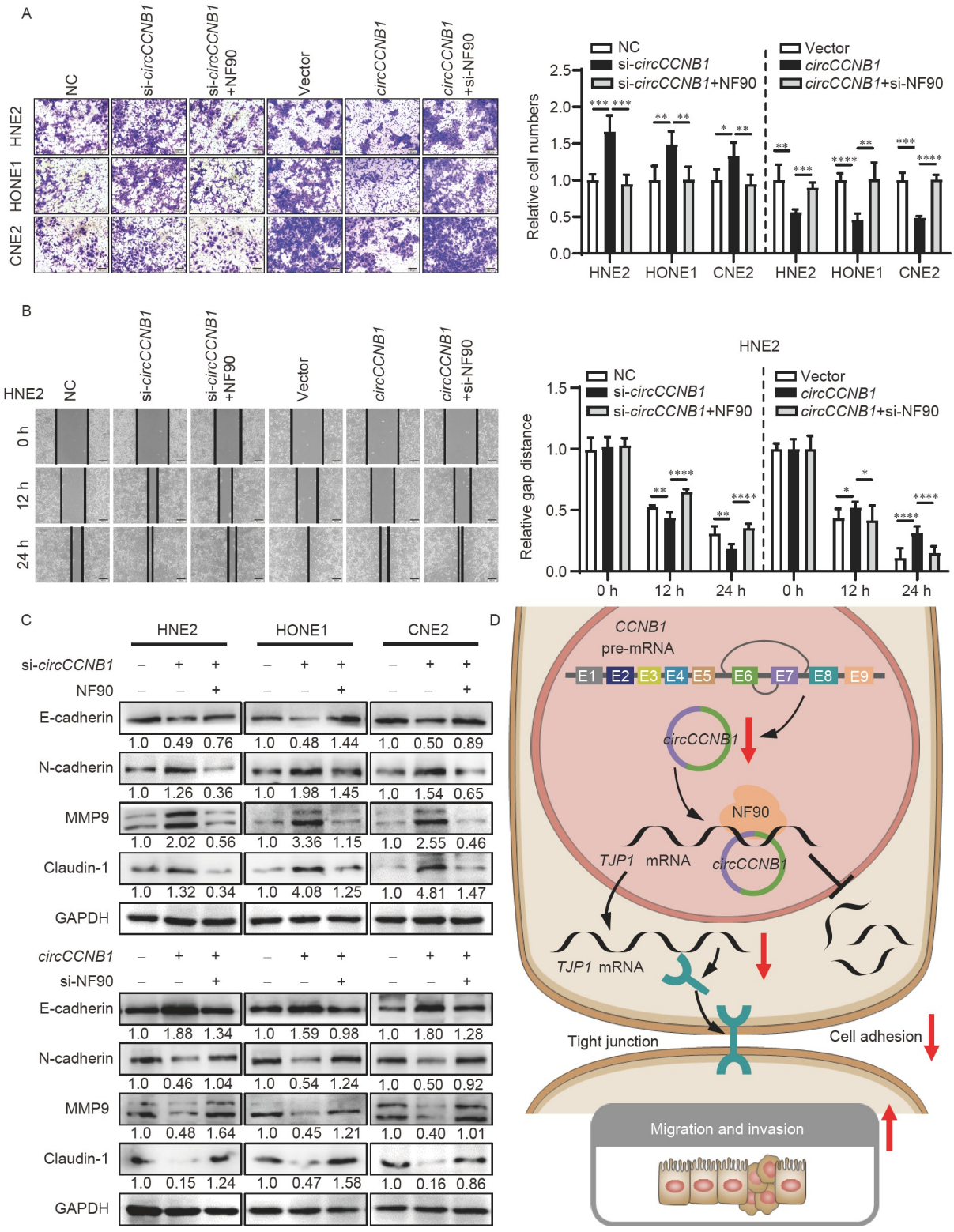

Figure 7 *circCCNB1* inhibits NPC migration and invasion through NF90. A, The invasive capability was assessed in HNE2, HONE1, and CNE2 cells after co-transfection *circCCNB1* siRNA and NF90 overexpression vector, or *circCCNB1* overexpression vector and NF90 siRNA by transwell assays, NF90 participated in the effectors of *circCCNB1* on NPC cell invasive capability. (*, $P<0.05$; **, $P<0.01$; ***, $P<0.001$; ****, $P<0.0001$). B, The migration capability was assessed in HNE2 cells after co-transfection *circCCNB1* siRNA and NF90 overexpression vector, or *circCCNB1* overexpression vector and NF90 siRNA by wound healing assays. NF90 participated in the effectors of *circCCNB1* on NPC cell migration capability. (*, $P<0.05$; **, $P<0.01$; ****, $P<0.0001$). C, The expression level of E-cadherin, N-cadherin, MMP9 and Claudin-1 were assessed by Western blotting assays in HNE2, HONE1, and CNE2 cells after co-transfection *circCCNB1* siRNA and NF90 overexpression vector, or *circCCNB1* overexpression vector and NF90 siRNA. D, Schematic illustration of the inhibition of NPC migration and invasion by *circCCNB1* through binding with NF90 and *TJP1* mRNA.

junctions (Ding et al., 2018; Ke et al., 2018; Liu et al., 2017; Mattern et al., 2019; Wu et al., 2017). This study uncovered a novel mechanism; *circCCNB1* is a positive post-transcriptional regulator of TJP1 that might inhibit EMT and metastasis in NPC.

NF90 is an RNA-binding protein that is encoded by *ILF3*. *ILF3* encodes two proteins with different molecular weights, namely NF90 and NF110 (Wu et al., 2019). As an RNA-binding protein, NF90 is involved in tumor progression mainly by affecting RNA metabolism by binding to RNA, including RNA production, transportation, stability, and translation (Ao et al., 2020; Ding et al., 2020; Jiang et al., 2015; Kuwano et al., 2010; Song et al., 2017). Instead of altered expression, NF90 exerts its function by being closely related to its bound mRNA (Wen et al., 2018). The expression and function of NF90 in NPC warrants further exploration to confirm and expand these findings. In this study, we demonstrated that the ability of NF90 to regulate *TJP1* mRNA stability was regulated by *circCCNB1*. Although *circCCNB1* did not affect the expression of NF90, the interaction between *circCCNB1* and NF90 enhanced the stability of *TJP1* mRNA. Therefore, further studies are needed to examine the concrete mechanism of *TJP1* mRNA stabilization regulated by *circCCNB1*.

In summary, this study demonstrates that *circCCNB1* is lowly expressed at low levels in NPC and is associated with the migration and invasion of NPC. Mechanistically, *circCCNB1* interacts with NF90 and subsequently promotes binding between NF90 and *TJP1* mRNA, leading to the upregulation of *TJP1* mRNA stability. We elucidated a new regulatory mechanism of *circCCNB1* in NPC migration and invasion that may provide potential markers and targets for the diagnosis and treatment of patients with NPC.

MATERIALS AND METHODS

Tissue samples

A total of 23 NPC clinical tissues and 10 non-cancerous nasopharyngeal epithelial tissues with chronic nasopharyngitis were collected from the Second Xiangya Hospital (Changsha, China; Table S1 in Supporting Information). The procedure was approved by the Ethics Committee of Central South University (Changsha, China). RNA was extracted with TRIzol reagent (Invitrogen, USA) and the expression of *circCCNB1* was detected by RT-qPCR.

Cell lines and transfection

Human NPC cell lines (HNE2, CNE2, HONE1, HK1, CNE1, 6-10B, and HNE1) and immortalized normal nasopharyngeal epithelial NP69 cells were obtained from the Cell Center of the Central South University (Changsha, China). Cells were cultured at 37°C in an incubator with 5% carbon dioxide (CO_2) in the Roswell Park Memorial Institute (RPMI) 1640 (Life Technologies, USA) supplemented with 10% fetal bovine serum (FBS; Gibco, USA) and 1% penicillin/streptomycin (Life Technologies).

To overexpress *circCCNB1*, exons 6 and 7 of *CCNB1* were reverse-amplified and cloned into pcDNA3.1 (+) circRNA mini vector (Baylor College of Medicine, USA), which contain tandem repeat sequences to aid circRNA looping at both ends of the inserted sequence. The NF90 overexpression vector (pCMV3-NF90-Flag) was purchased from the Sino Biological Company (Beijing, China). siRNAs according to *circCCNB1*, TJP1, or NF90 were designed to specifically knock them down. Hiperfect Reagent (Qiagen, Shanghai, China) was used for siRNA transfection and Neofect Reagent (Qiagen) was used to transfect the overexpression vectors.

RNA extraction and RT-qPCR

Total RNA was extracted using the TRIzol reagent (Invitrogen). Then, 1 μg of RNA was transcribed into cDNA using HiScript II Q RT SuperMix for RT-qPCR (+gDNA wiper) kit (Vazyme, Nanjing, China), and RT-qPCR was performed using 2x SYBR Green qPCR Master Mix kit (Biomake, Changsha, China) to detect the relative expression of genes. Relative primers were synthesized using Tsingke (Beijing, China), and the sequences are shown in Table S4 in Supporting Information.

Protein extraction and Western blotting

Cells were lysed with a RIPA lysis buffer plus cocktail (Beyotime, Shanghai, China) after transfection. The protein lysates were sonicated and centrifuged, the supernatant was collected, and its concentration was determined using the Pierce BCA Protein Assay Kit (Thermo Fisher Scientific, USA) for Western blotting. Then, protein lysates were separated on a 10% sodium dodecyl sulfate-polyacrylamide gel (SDS-PAGE) at 80 V/40 min and 120 V/60 min, and the proteins were transferred to polyvinylidene fluoride (PVDF) membranes (Millipore, USA) at 100 V for 90 min. The membrane was blocked with 5% bovine serum albumin (BSA) (Beyotime) for 1 h at room temperature and then incubated with primary antibodies at 4°C for 12–14 h. Then, the membrane was washed with 1×phosphate-buffered saline (PBS; Beyotime) three times at room temperature and incubated with secondary antibodies for 2 h at room temperature. Signals were detected using an Ultra High Sensitivity ECL Kit (New Cell & Molecular Biotech Co). The antibodies used are listed in Table S5 in Supporting Information.

Actinomycin D treatment

Actinomycin D (Sigma-Aldrich, USA) was used to detect RNA stability. NPC cells were treated with actinomycin D at a final concentration of 2 μg mL^{-1} and RNA was collected for RT-qPCR experiments. Semi-log plots were used to determine the decay of mRNA, and all data were normalized using $\log_2$.

Transwell assay

Transwell assays were performed to verify the invasive capacity of the cells. Matrigel (BD Biosciences, USA) was diluted with RPMI 1640, and 20 μL of the diluted Matrigel was added to the Transwell chambers (8-mm pores; Corning, USA) and incubated at 37°C for 2 h. Then, cells were counted and 2×10^4 cells were diluted to 200 μL with serum-free RPMI 1640 medium, added to the upper chamber, and 800 μL culture medium with 20% FBS was added to the well under the chamber and incubated at 37°C for 48 h, fixed with 4% paraformaldehyde (Beyotime), and stained with 0.1% crystal violet (Beyotime). Images were captured using an Olympus BX51 fluorescence microscope (Olympus, Japan), and the cells on the bottom surface of the chamber were counted.

Wound healing assay

A wound healing assay was performed to verify migration capacity. The plates were scratched with 10 μL pipette tips and cultured at 37°C. Images were captured at 0, 12, and 24 h after scratching, and gap distances were analyzed using Image Pro Plus v.6.0 software.

MTT assay

The MTT assay was performed to verify the proliferation capacity of the cells. Cells were counted, and 800 cells were diluted in 200 μL culture medium with 10% FBS and added to a 96-well plate. Then, 20 μL of MTT was added to each well after 6 h and 1–5 d, and the plate was incubated at 37°C for 4 h. Then, the liquid was discarded, 200 μL of dimethyl sulfoxide (DMSO; Beyotime) was added, and the absorbance values were detected at a wavelength of 490 nm using an enzyme-labeled instrument (Molecular Devices, USA).

Colony formation assay

Colony formation assay was performed to verify the proliferative capacity of the cells. Cells were counted and 800 were diluted to 1,000 μL culture medium with 10% FBS was added to a 6-well plate. Cells were incubated at 37°C for 5 d, fixed with 4% paraformaldehyde (Beyotime), and stained with 0.1% crystal violet (Beyotime). Images were captured and cell colonies in the wells were counted.

LC-MS/MS

Cells were harvested and lysed with a lysate (8 mol L^{-1} urea, 100 mmol L^{-1} dithiothreitol (DTT), 50 mmol L^{-1} ammonium bicarbonate (NH_4HCO_3), and cocktail (Beyotime)). The protein lysates were sonicated and centrifuged, the supernatant was collected, and its concentration was determined using the Bradford method. Then, DTT (0.1 mol L^{-1}) was added to 100 μg of protein to make the final DTT concentration 5 mmol L^{-1}. This solution was incubated in the dark at 56°C for 1 h and 0.1 mol L^{-1} iodoacetamide (IAA; Sigma-Aldrich) was added to obtain a final IAA concentration of 5 mmol L^{-1}, and further incubated in the dark at room temperature for 30 min. Later, DTT (0.1 mol L^{-1}) was added again to make the final DTT concentration 5 mmol L^{-1}, which was incubated in the dark at room temperature for 30 min to neutralize IAA. The solution was then diluted eight times with 50 mmol L^{-1} NH_4HCO_3 and 0.1 mol L^{-1} calcium chloride ($CaCl_2$; Sigma-Aldrich) was added to make the final $CaCl_2$ concentration to 1 mmol L^{-1}. Trypsin (1 μg) was then added to the solution and incubated for 18 h at 37°C. Trifluoroacetic acid (TFA; Sigma-Aldrich) was added at a final concentration of 1%. The sample was centrifuged, and the supernatant was desalted with Zip Tip C18, washed with 0.1% formic acid (FA; Sigma-Aldrich), resuspended in 80% acetonitrile (ACN; Sigma-Aldrich), and concentrated using a freeze-vacuum desiccator (Labconco Corporation, USA). The protein concentration was determined, and 1 μg of the sample was analyzed using Nano-LC LTQ Orbitrap EDT mass spectrometry (Bruker Daltonic, USA).

circRIP assay

Cells were transfected with biotin-labeled probes, harvested, and lysed with 1 mL lysate (working fluid was composed of 2 mL of 100 mmol L^{-1} Tris-hydrogen chloride (Tris-HCl; pH=8.0), 5 mL of 1 mmol L^{-1} sodium chloride (NaCl), 1 mL of 25 mmol L^{-1} magnesium chloride ($MgCl_2$), 2 mL of 10% SDS (Beyotime)), and an RNase inhibitor (Beyotime). The samples were incubated at 4°C for 10 min and then centrifuged again. The supernatant was collected and 50 μL was used as input, while the remaining was incubated with streptavidin Dynabeads (Thermo Fisher Scientific) for 2 h at room temperature. Then, 500 μL lysate was used to wash the beads three times, followed by the addition of 200 μL lysate with RNase inhibitor to resuspend the beads. RNA was extracted using a TRIzol reagent and analyzed using RT-qPCR.

RNA pull-down assay

Cells were transfected with biotin-labeled probes targeting the *circCCNB1* splicing sites, harvested, and lysed with 1 mL RIP buffer. Working fluid was composed of 7.5 mmol L^{-1} potassium chloride (KCl), 25 mmol L^{-1} Tris-HCl (pH=7.4), 0.5 mmol L^{-1} DTT, and 0.5% NP40 (Beyotime) with a protease inhibitor cocktail. The samples were incubated at 4°C for 2 h, centrifuged, and the supernatant was collected. Then, 50 μL of the supernatant was taken as the input, and the remaining was incubated with streptavidin Dynabeads for 2 h at room temperature. Subsequently, 1 mL of RIP buffer was used to wash the beads six times, and 50 μL of RIP buffer was used to resuspend the beads. Proteins enriched in the beads were denatured in boiling water and detected using Western blotting.

RIP assay

The RIP assay was performed using a RIP kit (Millipore). Cells were incubated at 4°C for 10 min, centrifuged, and the supernatant was collected, from which 10 μL was used as the input. The beads were washed with 500 μL of RIP wash buffer, incubated with 3 μg of antibody at room temperature for 30 min, and then spun slowly. The remaining supernatant and 900 μL of RIP buffer were added, incubated at 4°C overnight, and then spun slowly. The beads were washed with RIP wash buffer six times, 150 μL proteinase K buffer was added, and the beads were incubated at 55°C for 30 min. The supernatant was collected and RNA was extracted with phenol-chloroform (Sigma-Aldrich) and analyzed by RT-qPCR.

Fluorescence *in situ* hybridization

Cells were fixed with 200 μL preheated 4% paraformaldehyde for 30 min at 37°C. The cell membranes were broken with 0.25% Triton-100 for 15 min, washed with PBS for 3 times, blocked with 5% BSA for 30 min at room temperature, and then incubated with digoxin-labeled probe targeting *circCCNB1* splicing sites at 37°C overnight after prehybridization for 3 h. They were then washed twice with 2×saline sodium citrate (SSC; Beyotime), once with 0.5×SSC, and twice with 0.2×SSC buffer. Biotinylated mouse anti-digoxin was then added for 1 h (Boster, USA), incubated with secondary antibodies at 37°C for 1 h in the dark, and washed with PBS three times. Subsequently, 4′,6-diamidino-2-phenylindole (DAPI; Beyotime) was used to stain the nucleus for 20 min at room temperature in the dark, washed with PBS for 2 times, sealed, and imaged using a confocal microscope (PerkinElmer, USA).

Immunofluorescence

Cells were fixed with 200 μL preheated 4% paraformaldehyde for 30 min at 37°C, the cell membranes were broken with 0.25% Triton-100 for 15 min, washed with PBS three times, blocked with 5% BSA for 30 min at room temperature, and incubated with antibodies at 4°C overnight. They were then washed with PBS four 4 times, incubated with secondary antibodies at 37°C for 1 h in the dark, and washed with PBS four times. Nucleus were stained with DAPI for 20 min at room temperature in the dark, and the cells were washed twice with PBS, sealed, and imaged using a confocal microscope (PerkinElmer, USA).

Statistical analyses

GraphPad Prism 8 software was used for all statistical analyses, and Student's *t*-test was used to analyze the differences between pairs of independent groups. The *P*-values<0.05 were considered to be statistically significant (*, $P<0.05$; **, $P<0.01$; ***, $P<0.001$; ****, $P<0.0001$). Image Pro Plus v.6.0 was used to analyze wound healing and transwell assays. ImageJ software was used to analyze the images from Western blotting.

Availability of data and materials

All data that support the findings of this study are available from the corresponding authors upon reasonable request.

Compliance and ethics *The author(s) declare that they have no conflict of interest. The present study was approved by the Ethics Committee of Central South University.*

Acknowledgements *This work was supported by the National Natural Science Foundation of China (82002239, 82072374 and 82073135), the Overseas Expertise Introduction Project for Discipline Innovation (111 Project, 111-2-12), the Natural Science Foundation of Hunan Province (2021JJ41043 and 2021JJ30897), Central South University Graduate Research and Innovation Project (2021zzts0310). We thank Prof. Li Yong for providing pcDNA3.1(+) CircRNA Mini Vectors.*

References

Ao, X., Li, X., Chen, Y., Zang, Z., Guo, W., and Liang, J. (2020). TMEM98 mRNA promotes proliferation and invasion of gastric cells by directly interacting with NF90 protein. Cell Biol Int 44, 1820–1830.

Aussem, A., de Morais, S.R., and Corbex, M. (2012). Analysis of nasopharyngeal carcinoma risk factors with Bayesian networks. Artif Intell Med 54, 53–62.

Chen, E.B., Qin, X., Peng, K., Li, Q., Tang, C., Wei, Y.C., Yu, S., Gan, L., and Liu, T.S. (2019). HnRNPR-CCNB1/CENPF axis contributes to gastric cancer proliferation and metastasis. Aging 11, 7473–7491.

Ding, D., Huang, H., Li, Q., Yu, W., Wang, C., Ma, H., Wu, J., Dang, Y., Yu, L., and Jiang, W. (2020). NF90 stabilizes cyclin E1 mRNA through phosphorylation of NF90-Ser382 by CDK2. Cell Death Discov 6, 3.

Ding, N.H., Zhang, L., Xiao, Z., Rong, Z.X., Li, Z., He, J., Chen, L., Ou, D. M., Liao, W.H., and Sun, L.Q. (2018). NEK4 kinase regulates EMT to promote lung cancer metastasis. J Cell Mol Med 22, 5877–5887.

Fan, C., Wang, J., Tang, Y., Zhang, S., Xiong, F., Guo, C., Zhou, Y., Li, Z., Li, X., Li, Y., et al. (2020). Upregulation of long non-coding RNA

LOC284454 may serve as a new serum diagnostic biomarker for head and neck cancers. BMC Cancer 20, 917.
Fan, C., Qu, H., Xiong, F., Tang, Y., Tang, T., Zhang, L., Mo, Y., Li, X., Guo, C., Zhang, S., et al. (2021a). CircARHGAP12 promotes nasopharyngeal carcinoma migration and invasion via ezrin-mediated cytoskeletal remodeling. Cancer Lett 496, 41–56.
Fan, C., Zhang, S., Gong, Z., Li, X., Xiang, B., Deng, H., Zhou, M., Li, G., Li, Y., Xiong, W., et al. (2021b). Emerging role of metabolic reprogramming in tumor immune evasion and immunotherapy. Sci China Life Sci 64, 534–547.
Fan, C.M., Wang, J.P., Tang, Y.Y., Zhao, J., He, S.Y., Xiong, F., Guo, C., Xiang, B., Zhou, M., Li, X.L., et al. (2019). *circMAN1A2* could serve as a novel serum biomarker for malignant tumors. Cancer Sci 110, 2180–2188.
Fang, L., Du, W.W., Lyu, J., Dong, J., Zhang, C., Yang, W., He, A., Kwok, Y.S.S., Ma, J., Wu, N., et al. (2018). Enhanced breast cancer progression by mutant p53 is inhibited by the circular RNA circ-Ccnb1. Cell Death Differ 25, 2195–2208.
Fang, L., Du, W.W., Awan, F.M., Dong, J., and Yang, B.B. (2019). The circular RNA circ-Ccnb1 dissociates Ccnb1/Cdk1 complex suppressing cell invasion and tumorigenesis. Cancer Lett 459, 216–226.
Gao, X., Xia, X., Li, F., Zhang, M., Zhou, H., Wu, X., Zhong, J., Zhao, Z., Zhao, K., Liu, D., et al. (2021). Circular RNA-encoded oncogenic E-cadherin variant promotes glioblastoma tumorigenicity through activation of EGFR-STAT3 signalling. Nat Cell Biol 23, 278–291.
Ge, J., Wang, J., Xiong, F., Jiang, X., Zhu, K., Wang, Y., Mo, Y., Gong, Z., Zhang, S., He, Y., et al. (2021). Epstein-Barr virus-encoded circular RNA circBART2.2 promotes immune escape of nasopharyngeal carcinoma by regulating PD-L1. Cancer Res 81, 5074–5088.
Hildesheim, A., and Wang, C.P. (2012). Genetic predisposition factors and nasopharyngeal carcinoma risk: a review of epidemiological association studies, 2000–2011. Semin Cancer Biol 22, 107–116.
Jiang, W., Huang, H., Ding, L., Zhu, P., Saiyin, H., Ji, G., Zuo, J., Han, D., Pan, Y., Ding, D., et al. (2015). Regulation of cell cycle of hepatocellular carcinoma by NF90 through modulation of cyclin E1 mRNA stability. Oncogene 34, 4460–4470.
Jiang, X., Deng, X., Wang, J., Mo, Y., Shi, L., Wei, F., Zhang, S., Gong, Z., He, Y., Xiong, F., et al. (2022). BPIFB1 inhibits vasculogenic mimicry via downregulation of GLUT1-mediated H3K27 acetylation in nasopharyngeal carcinoma. Oncogene 41, 233–245.
Karthi, S., Rajeshwari, M., Francis, A., Saravanan, M., Varalakshmi, P., Houlden, H., Thangaraj, K., and Ashokkumar, B. (2017). 3′-UTR SNP rs2229611 in G6PC1 affects mRNA stability, expression and Glycogen Storage Disease type-Ia risk. Clin Chim Acta 471, 46–54.
Ke, J., Shao, W., Jiang, Y., Xu, J., Li, F., and Qin, J. (2018). MicroRNA-103 regulates tumorigenesis in colorectal cancer by targeting ZO-1. Mol Med Report 17, 783–788.
Kuwano, Y., Pullmann Jr., R., Marasa, B.S., Abdelmohsen, K., Lee, E.K., Yang, X., Martindale, J.L., Zhan, M., and Gorospe, M. (2010). NF90 selectively represses the translation of target mRNAs bearing an AU-rich signature motif. Nucleic Acids Res 38, 225–238.
Li, P., Zhu, K., Mo, Y., Deng, X., Jiang, X., Shi, L., Guo, C., Zhang, W., Zeng, Z., Li, G., et al. (2021). Research progress of circRNAs in head and neck cancers. Front Oncol 11, 616202.
Liang, W.C., Wong, C.W., Liang, P.P., Shi, M., Cao, Y., Rao, S.T., Tsui, S. K.W., Waye, M.M.Y., Zhang, Q., Fu, W.M., et al. (2019). Translation of the circular RNA circβ-catenin promotes liver cancer cell growth through activation of the Wnt pathway. Genome Biol 20, 84.
Liu, Z., Zou, D., Yang, X., Xue, X., Zuo, L., Zhou, Q., Hu, R., and Wang, Y. (2017). Melatonin inhibits colon cancer RKO cell migration by downregulating Rho-associated protein kinase expression via the p38/MAPK signaling pathway. Mol Med Rep 16, 9383–9392.
Mattern, J., Roghi, C.S., Hurtz, M., Knäuper, V., Edwards, D.R., and Poghosyan, Z. (2019). ADAM15 mediates upregulation of Claudin-1 expression in breast cancer cells. Sci Rep 9, 12540.
Mo, Y., Wang, Y., Zhang, S., Xiong, F., Yan, Q., Jiang, X., Deng, X., Wang, Y., Fan, C., Tang, L., et al. (2021). Circular RNA circRNF13 inhibits proliferation and metastasis of nasopharyngeal carcinoma via SUMO2. Mol Cancer 20, 112.
Ouhara, K., Munenaga, S., Kajiya, M., Takeda, K., Matsuda, S., Sato, Y., Hamamoto, Y., Iwata, T., Yamasaki, S., Akutagawa, K., et al. (2018). The induced RNA-binding protein, HuR, targets 3′-UTR region of IL-6 mRNA and enhances its stabilization in periodontitis. Clin Exp Immunol 192, 325–336.
Ouyang, J., Zhang, Y., Xiong, F., Zhang, S., Gong, Z, Yan, Q, He, Y., Wei, F., Zhang, W., Zhou, M., et al. (2021a). The role of alternative splicing in human cancer progression. Am J Cancer Res 11, 4642–4667.
Ouyang, J., Zhong, Y., Zhang, Y., Yang, L., Wu, P., Hou, X., Xiong, F., Li, X., Zhang, S., Gong, Z., et al. (2021b). Long non-coding RNAs are involved in alternative splicing and promote cancer progression. Br J Cancer doi:10.1038/s41416-021-01600-w.
Qu, H., Fan, C., Chen, M., Zhang, X., Yan, Q., Wang, Y., Zhang, S., Gong, Z., Shi, L., Li, X., et al. (2021). Recent advances of fluorescent biosensors based on cyclic signal amplification technology in biomedical detection. J Nanobiotechnol 19, 403.
Qu, H., Chen, M., Ge, J., Zhang, X., He, S., Xiong, F., Yan, Q., Zhang, S., Gong, Z., Guo, C., et al. (2022). A fluorescence strategy for circRNA quantification in tumor cells based on T7 nuclease-assisted cycling enzymatic amplification. Anal Chim Acta 1189, 339210.
Ren, D., Hua, Y., Yu, B., Ye, X., He, Z., Li, C., Wang, J., Mo, Y., Wei, X., Chen, Y., et al. (2020). Predictive biomarkers and mechanisms underlying resistance to PD1/PD-L1 blockade cancer immunotherapy. Mol Cancer 19, 19.
Runkle, E.A., and Mu, D. (2013). Tight junction proteins: from barrier to tumorigenesis. Cancer Lett 337, 41–48.
Sanger, H.L., Klotz, G., Riesner, D., Gross, H.J., and Kleinschmidt, A.K. (1976). Viroids are single-stranded covalently closed circular RNA molecules existing as highly base-paired rod-like structures. Proc Natl Acad Sci USA 73, 3852–3856.
Saw, P.E., Xu, X., Chen, J., and Song, E.W. (2021). Non-coding RNAs: the new central dogma of cancer biology. Sci China Life Sci 64, 22–50.
Song, D., Huang, H., Wang, J., Zhao, Y., Hu, X., He, F., Yu, L., and Wu, J. (2017). NF90 regulates PARP1 mRNA stability in hepatocellular carcinoma. Biochem Biophys Res Commun 488, 211–217.
Tang, L., Xiong, W., Zhang, L., Wang, D., Wang, Y., Wu, Y., Wei, F., Mo, Y., Hou, X., Shi, L., et al. (2021). circSETD3 regulates MAPRE1 through miR-615-5p and miR-1538 sponges to promote migration and invasion in nasopharyngeal carcinoma. Oncogene 40, 307–321.
Wang, J., Ge, J., Wang, Y., Xiong, F., Guo, J., Jiang, X., Zhang, L., Deng, X., Gong, Z., Zhang, S., et al. (2022a). EBV miRNAs BART11 and BART17-3p promote immune escape through the enhancer-mediated transcription of PD-L1. Nat Commun 13, 866.
Wang, Y., Bao, Y., Zhang, S., and Wang, Z. (2020). Splicing dysregulation in cancer: from mechanistic understanding to a new class of therapeutic targets. Sci China Life Sci 63, 469–484.
Wang, Y., Mo, Y., Peng, M., Zhang, S., Gong, Z., Yan, Q., Tang, Y., He, Y., Liao, Q., Li, X., et al. (2022b). The influence of circular RNAs on autophagy and disease progression. Autophagy 18, 240–253.
Wang, Y., Yan, Q., Mo, Y., Liu, Y., Wang, Y., Zhang, S., Guo, C., Wang, F., Li, G., Zeng, Z., et al. (2022c). Splicing factor derived circular RNA circCAMSAP1 accelerates nasopharyngeal carcinoma tumorigenesis via a SERPINH1/c-Myc positive feedback loop. Mol Cancer 21, 62.
Wen, X., Liu, X., Mao, Y.P., Yang, X.J., Wang, Y.Q., Zhang, P.P., Lei, Y., Hong, X.H., He, Q.M., Ma, J., et al. (2018). Long non-coding RNA DANCR stabilizes HIF-1α and promotes metastasis by interacting with NF90/NF45 complex in nasopharyngeal carcinoma. Theranostics 8, 5676–5689.
Wu, J., Zhou, X.J., Sun, X., Xia, T.S., Li, X.X., Shi, L., Zhu, L., Zhou, W. B., Wei, J.F., and Ding, Q. (2017). RBM38 is involved in TGF-β-induced epithelial-to-mesenchymal transition by stabilising zonula occludens-1 mRNA in breast cancer. Br J Cancer 117, 675–684.
Wu, P., Mo, Y., Peng, M., Tang, T., Zhong, Y., Deng, X., Xiong, F., Guo, C., Wu, X., Li, Y., et al. (2020a). Emerging role of tumor-related functional peptides encoded by lncRNA and circRNA. Mol Cancer 19, 22.

Wu, T.H., Shi, L., Lowe, A.W., Nicolls, M.R., and Kao, P.N. (2019). Inducible expression of immediate early genes is regulated through dynamic chromatin association by NF45/ILF2 and NF90/NF110/ILF3. PLoS ONE 14, e0216042.

Wu, Y., Wang, D., Wei, F., Xiong, F., Zhang, S., Gong, Z., Shi, L., Li, X., Xiang, B., Ma, J., et al. (2020b). EBV-miR-BART12 accelerates migration and invasion in EBV-associated cancer cells by targeting tubulin polymerization-promoting protein 1. FASEB J 34, 16205–16223.

Xia, X., Li, X., Li, F., Wu, X., Zhang, M., Zhou, H., Huang, N., Yang, X., Xiao, F., Liu, D., et al. (2019). A novel tumor suppressor protein encoded by circular AKT3 RNA inhibits glioblastoma tumorigenicity by competing with active phosphoinositide-dependent Kinase-1. Mol Cancer 18, 131.

Xie, B.S., Wang, Y.Q., Lin, Y., Zhao, C.C., Mao, Q., Feng, J.F., Cao, J.Y., Gao, G.Y., and Jiang, J.Y. (2018). Circular RNA expression profiles alter significantly after traumatic brain injury in rats. J Neurotrauma 35, 1659–1666.

Xie, L., Shi, F., Li, Y., Li, W., Yu, X., Zhao, L., Zhou, M., Hu, J., Luo, X., Tang, M., et al. (2020). Drp1-dependent remodeling of mitochondrial morphology triggered by EBV-LMP1 increases cisplatin resistance. Sig Transduct Target Ther 5, 56.

Xiong, F., Zhu, K., Deng, S., Huang, H., Yang, L., Gong, Z., Shi, L., He, Y., Tang, Y., Liao, Q., et al. (2021). AFAP1-AS1: a rising star among oncogenic long non-coding RNAs. Sci China Life Sci 64, 1602–1611.

Ye, J., Jin, H., Pankov, A., Song, J.S., and Blelloch, R. (2017). NF45 and NF90/NF110 coordinately regulate ESC pluripotency and differentiation. RNA 23, 1270–1284.

Yu, A.Q., Wang, Z.X., Wu, W., Chen, K.Y., Yan, S.R., and Mao, Z.B. (2019). Circular RNA CircCCNB1 sponges micro RNA-449a to inhibit cellular senescence by targeting CCNE2. Aging 11, 10220–10241.

Zeng, Z.Y., Huang, H.B., Zhang, W.L., Xiang, B., Zhou, M., Zhou, Y.H., Ma, J., Yi, M., Li, X.Y., Li, X.L., et al. (2011). Nasopharyngeal carcinoma: advances in genomics and molecular genetics. Sci China Life Sci 54, 966–975.

Zhang, L., Feng, T., and Spicer, L.J. (2018). The role of tight junction proteins in ovarian follicular development and ovarian cancer. Reproduction 155, R183–R198.

Zhao, J., Guo, C., Xiong, F., Yu, J., Ge, J., Wang, H., Liao, Q., Zhou, Y., Gong, Q., Xiang, B., et al. (2020). Single cell RNA-seq reveals the landscape of tumor and infiltrating immune cells in nasopharyngeal carcinoma. Cancer Lett 477, 131–143.

Zhong, Y., Du, Y., Yang, X., Mo, Y., Fan, C., Xiong, F., Ren, D., Ye, X., Li, C., Wang, Y., et al. (2018). Circular RNAs function as ceRNAs to regulate and control human cancer progression. Mol Cancer 17, 79.

Zhou, R., Wu, Y., Wang, W., Su, W., Liu, Y., Wang, Y., Fan, C., Li, X., Li, G., Li, Y., et al. (2018). Circular RNAs (circRNAs) in cancer. Cancer Lett 425, 134–142.

Zhu, K., Hu, X., Chen, H., Li, F., Yin, N., Liu, A.L., Shan, K., Qin, Y.W., Huang, X., Chang, Q., et al. (2019). Downregulation of circRNA DMNT3B contributes to diabetic retinal vascular dysfunction through targeting miR-20b-5p and BAMBI. Ebiomedicine 49, 341–353.

Zhu, K., Ge, J., He, Y., Li, P., Jiang, X., Wang, J., Mo, Y., Huang, W., Gong, Z., Zeng, Z., et al. (2021). Bioinformatics analysis of the signaling pathways and genes of gossypol induce death of nasopharyngeal carcinoma cells. DNA Cell Biol 40, 1052–1063.

SUPPORTING INFORMATION

The supporting information is available online at https://doi.org/10.1007/s11427-021-2089-8. The supporting materials are published as submitted, without typesetting or editing. The responsibility for scientific accuracy and content remains entirely with the authors.